

MT-MADRAS brightness temperature analysis for terrain characterization and land surface microwave emissivity estimation

C. Suresh Raju*, Tinu Antony, Nizy Mathew, K. N. Uma and K. Krishna Moorthy

Space Physics Laboratory, Vikram Sarabhai Space Centre, ISRO, Thiruvananthapuram 695 022, India

This article reports the potential of the ‘MADRAS’ payload on-board the Megha-Tropiques satellite for land surface studies. The analysis has been divided into two parts as application of MADRAS data for studying the land surface properties and estimation of microwave emissivity directly from MADRAS brightness temperature (TB) data by applying an in-house developed Microwave Radiative Transfer Computation Code. The derived emissivity is further used to characterize the microwave emissivity of different land surface classes. The polarization difference (PD) parameters, the difference between horizontal (*H*-) and vertical (*V*-) polarization of TBs at 18 and 36 GHz clearly discern surface features of different surface classes such as deserts, arid/semi-arid and vegetated regions. Land surface microwave emissivity for MADRAS channels is derived on a global basis. These are inter-compared with the emissivity derived from the operational TRMM Microwave Imager and are in reasonably good agreement. The analysis based on emissivity shows spectral variation for different surface classes.

Keywords: Land-surface microwave emissivity, MADRAS payload, Megha-Tropiques mission, Microwave radiometry.

Introduction

THE meteorological and climatic processes over the tropics play a vital role in regulating global weather and climate, in terms of circulation, and transfer of energy and momentum. The measurements of water and energy budget of the tropical atmosphere with reliable statistics at appropriate space–time scales are essential to describe the evolution of large-scale systems such as monsoons and cyclones. Several microwave satellites (for example, TRMM, AMSU, MLS and HSB) are operational for simultaneous observations of water vapour, clouds, precipitation and radiative flux. The Megha-Tropiques (MT) satellite, an Indo-French collaborative satellite programme, is a unique mission with sampling focused over

the intertropical zone to account for the large space–time variability of the tropical phenomena. The objective of the MT mission is to study the water cycle and evaluate its influence on the energy budget, with a specific focus on the analysis of the life cycle of tropical convection.

MT was successfully launched on 12 October 2011 using the Indian Polar Satellite Launch Vehicle (PSLV C-12) and was placed at ~865 km altitude in a circular orbit with 20° inclination. This orbital configuration provides the advantage of making frequent sampling of the tropical region between 28°N and 28°S. It can even observe some locations five/six times a day, which enables the study of the large spatio-temporal variability of the tropical phenomena at high spatial and temporal resolutions. Generally, the overpasses are at different local times of the day, which provides unbiased daily means of atmospheric and cloud parameters unlike the polar satellites. There are two microwave payloads on-board MT: (1) MADRAS (Microwave Analysis and Detection of Rain and Atmospheric Systems) – a conical scan microwave imager to measure precipitation, total columnar water vapour and cloud parameters; (2) SAPHIR (Sondeur Atmosphérique du Profil d’Humidité en Intertropicale par Radiométrie) – a cross-track microwave sounder to estimate vertical structure of atmospheric water vapour.

Over the oceanic region, satellite microwave radiometer measurements are effectively used for many atmospheric studies and routinely assimilated in NWP models for weather prediction. Relatively high land emissivity with large temporal variation and spatial heterogeneity, and coarse spatial resolution of sensors are the factors that limit the utility of microwave satellite remote sensing over the continent¹. The land surface emissivity depends on various surface parameters such as vegetation, surface roughness and soil moisture, and hence modelling emissivities (accounting to their large spatial and temporal variability) on a global scale is a real challenge². For the application of microwave radiometers for cloud and atmospheric studies over the continental region accurate surface emissivity measurements are essential^{3,4}. Efforts have been taken to estimate land surface emissivity

*For correspondence. (e-mail: c_sureshraj@vssc.gov.in)

directly from satellite observations so as to use, invert and assimilate microwave radiances over land^{5,6}. Apart from that, microwave emissivity estimate is useful to define the characteristics of different land surface classes and the temporal and spatial variations of land surface properties at regional and global scales. Land surface emissivities are also used for delineating wetlands, water-logged areas and flood-affected regions⁷. A database of microwave land surface emissivity climatology, derived directly from satellite observations on a global basis, has been made available^{4,5}.

This article highlights the utility of microwave imaging payload MADRAS on-board MT for studying the terrain characteristics using brightness temperature data, and estimation of surface emissivity and comparison of MT-derived emissivity with those from TRMM Microwave Imager (TMI).

Data and methodology

Data

MADRAS data: The level-1 brightness temperature (TB) data of MADRAS have been used for the present study. The MADRAS payload has been developed jointly by ISRO (India) and CNES (France). The payload design, characteristics and applications are detailed in the present issue. MADRAS is a dual (*H* and *V*) polarization microwave imager measuring radiance at five frequencies (18.7, 23.8, 36.5, 89 and 157 GHz), except for 23.8 GHz (*V* only). It is a conical scanning (~53° incidence angle), self-calibrating, total power radiometer which measures the brightness temperatures in latitudinal region of ~28°N to ~28°S. The first three channels (low-frequency channels) have spatial resolution of ~40 km. The 89 GHz channel has a resolution of ~10 km and for the 157 GHz channel it is ~6 km. Dual polarization measurements at 157 GHz is a unique feature of MADRAS.

TRMM Microwave imager data: TRMM is a joint mission by NASA (United States) and JAXA (Japan) with an objective to measure the rainfall and energy exchange in the tropical and subtropical regions. TRMM is placed in a low inclined orbit (35° inclination) having latitudinal coverage between 35°N and 35°S. TRMM passes over a given area at different local times of the day with a 42-day repeat cycle. TRMM Microwave Imager (TMI) is a conical scanning (at 53° incidence angle), which has nine channels operating at 10.7, 19.23, 21.3 (*V* only), 37 and 85 GHz (ref. 8). The key difference between MADRAS and TMI is that the latter has an additional low-frequency channel (10.7 GHz) which is more sensitive to soil moisture and land surface variability, whereas MADRAS has 157 GHz frequency which is more sensitive to cloud parameters.

Methodology for emissivity retrieval

The microwave emission received by the satellite radiometer has contributions from the Earth's surface and the intervening atmosphere. In order to separate out land surface contribution, microwave emission from the atmosphere has to be quantified. This is accomplished by applying the microwave radiative transfer calculations with the atmospheric profiles of pressure, temperature and humidity as inputs under clear-sky conditions. The microwave radiative transfer formulation in terms of the brightness temperature (T_B) over a flat lossy surface, for a non-scattering plane-parallel atmosphere for a given zenith angle, at a given polarization p (where p is polarization *H*- or *V*-) is given as

$$T_B(p, f) = (T_{\text{skin}} \times \epsilon(p, f) \times \Gamma) + (T_{\downarrow}(f) \times (1 - \epsilon(p, f)) \times \Gamma) + T_{\uparrow}(f), \quad (1)$$

where $T_B(p, f)$ is the satellite observed brightness temperature, $\epsilon(p, f)$ the surface emissivity at a frequency f . Γ is the net atmospheric transmissivity ($\Gamma = e^{-\alpha(0, H)/\mu}$, where H is the height of the satellite and μ is $\cos(\theta)$, θ is the incidence angle) and T_{skin} , $T_{\downarrow}(f)$ and $T_{\uparrow}(f)$ are the skin temperature, downwelling and upwelling brightness temperatures respectively.

Equation (1) leads to the land emissivity expression as

$$\epsilon(P, f) = \frac{T_B(P, f) - T_{\uparrow}(f) - T_{\downarrow}(f) \times \Gamma}{(T_{\text{skin}} - T_{\downarrow}(f)) \times \Gamma}. \quad (2)$$

$T_{\downarrow}(f)$ and $T_{\uparrow}(f)$ are numerically estimated using radiative transfer (RT) computation as

$$T_{\downarrow}(f) = \int T(z) [\kappa_a(z)/\mu] e^{-\tau(z, 0)/\mu} dz + T_{\text{csm}} e^{-\tau(0, H)/\mu},$$

and

$$T_{\uparrow}(f) = \int T(z) [\kappa_a(z)/\mu] e^{-\tau(z, H)/\mu} dz, \quad (3)$$

where $\kappa_a(z)$ is the atmospheric absorption at altitude z , $T(z)$ is the atmospheric temperature as a function of altitude, $\tau(z_0, z_1) = \int \kappa_a(z) dz$ is the atmospheric opacity from z_0 to z_1 , and T_{csm} is the cosmic background brightness temperature (considered to be ~2.7 K). RT computation describes the propagation of energy from the emission source to the sensor through a horizontally stratified atmospheric medium based on the physical principles responsible for emission, absorption and scattering of a signal, referred to jointly as extinction. When a radiation passes through a stratified atmosphere, each layer absorbs a fraction of the incident radiation and further re-emits, to maintain the local thermal equilibrium state of the layer. As radiation intensity emitted by each layer is independent of the temperature of the other layers, the total emission is obtained by adding the contribution from every layer. This RT equation basically contains attenuation, scatter-

ing and source functions under certain boundary conditions. As absorption and scattering are linear processes, the extinction coefficient (κ_e) may be expressed as the sum of an absorption coefficient (κ_a) and a scattering coefficient (κ_s) as

$$\kappa_e = \kappa_a + \kappa_s.$$

Limiting the RT computations for clear sky or non-scattering condition ($\kappa_s = 0$), absorption and emission are the leading physical processes in the microwave interaction with the atmospheric medium and the extinction is solely due to absorption ($\kappa_e = \kappa_a$). Water vapour and oxygen are the main atmospheric constituents that influence microwave absorption. Hence RT of microwaves through clear sky is modelled by integrating absorption due to each spectral line for both oxygen and water vapour^{9–12}. This is referred to as a line-by-line RT model. Extra correction term for absorption¹³ has also been added to account for the correction in the continuum. The total gaseous absorption coefficient is therefore given by

$$\kappa_a(f) = \kappa_{\text{H}_2\text{O}}(f) + \kappa_{\text{O}_2}(f) \quad \text{dB/km}, \quad (4)$$

where $\kappa_{\text{H}_2\text{O}}(f)$ and $\kappa_{\text{O}_2}(f)$ are absorption coefficients of water vapour and oxygen respectively. The atmospheric absorption coefficients are computed using atmospheric profiles of pressure (P), temperature (T) and water vapour density (ρ_w) derived from relative humidity (RH). These atmospheric parameters at different altitudes (37 levels, $1.5^\circ \times 1.5^\circ$ grid), and T_{skin} (surface temperature) are obtained from the European Center for Medium Range Weather Forecasting (ECMWF) reanalysis (<http://data-portal.ecmwf.in/data/d/interimdaily>). Cloudy pixels are removed from the analysis using the ECMWF cloud data product, METEOSAT images, KALPANA data¹⁴ and collocated SAPHIR data. The estimated uncertainty of pressure and temperature in ECMWF¹⁵ is 1–2 hPa and 1–2 K respectively, while that for relative humidity is $\sim 20\%$. For surface emissivity retrieval the methodology by Prigent *et al.*¹ has been adopted.

Results

MADRAS TB data of 9 December 2011 which were made available to the PIs of MT data utility programme, have been used in this study. The level-1 TB data from MADRAS have been analysed for studying various land surface features. The results are presented in the following subsections.

Land surface characterization using MADRAS TB data

The MADRAS channels at 18, 23 and 36 GHz are classified as low resolution (~ 40 km) channels, whereas 89

and 157 GHz (having spatial resolutions about 10 and 6 km respectively) are classified as medium and high resolution channels respectively. The TB maps for these MADRAS channels covering the intertropical region (figure is not shown) are generated. It is observed that continents and oceanic regions are well distinguishable in low resolution channels however, they are hardly distinguishable at higher frequencies. The 157 GHz channels are more sensitive to tropical atmosphere due to the absorption of water vapour as well as scattering by hydrometeors and cirrus clouds¹⁶.

Though MADRAS radiometer is designed to estimate the clouds and precipitation over the oceanic region, utilizing the potential of dual polarization measurements of these atmospheric window channels with significant sensitivity to surface variability, MADRAS data can effectively be used for land surface studies. The microwave emission at V - and H -polarizations has significant influence on surface roughness in the case of barren and desert land, whereas for vegetated and forest regions volume (diffuse) scattering dominates. The polarization difference (TBV–TBH) maps are derived for all MADRAS channels. Besides clear land–sea contrast, the polarization difference (PD) is more sensitive to surface variability over continental region. The gross and distinct features of the land, such as thick vegetation (Amazon forest), tropical forest, deserts and savannas of Africa, and deserts and grasslands of Australia could be clearly discerned. The savanna region adjoining the desert shows a moderate PD of 20–30 K whereas thick vegetated forest regions in Africa show very low PD < 5 K. Similar features have been observed over Australia where the savanna and desert regions are clearly distinguishable. The PD decreases with frequency and at 157 GHz, the PD values are very small and the land surface variability is hardly distinguishable.

As an example, the PD map (TBV–TBH) of the African continent at 18 GHz is shown in Figure 1 (left panel). To investigate the dependence of PD on biomass density and vegetation cover, the MODIS derived 16-day mean Normalized Difference Vegetation Index (NDVI) data are analysed (Figure 1, right panel). NDVI values are low (~ 0.1) over Sahara desert in Africa; however the PD values for this region range from 25 to 55 K. Deserts act as quasi-specular reflecting surfaces depending on the terrain roughness. The TB variation due to surface roughness at higher incidence angles (as in case of MADRAS, $\sim 53^\circ$) is relatively large for H -polarization than that for V -polarization. Some parts of the desert area, along the 20°N longitudinal sector, have the highest PD > 50 K, indicating very smooth surface which characterizes the presence of sand dunes. The desert areas around the sand dunes show lesser PD, ranging from ~ 30 to ~ 40 K. When the terrain is sparsely vegetated in the case of dry savanna, the land surface is also partly exposed. Thus in such regions the emission is from both vegetation and dry soil surface.

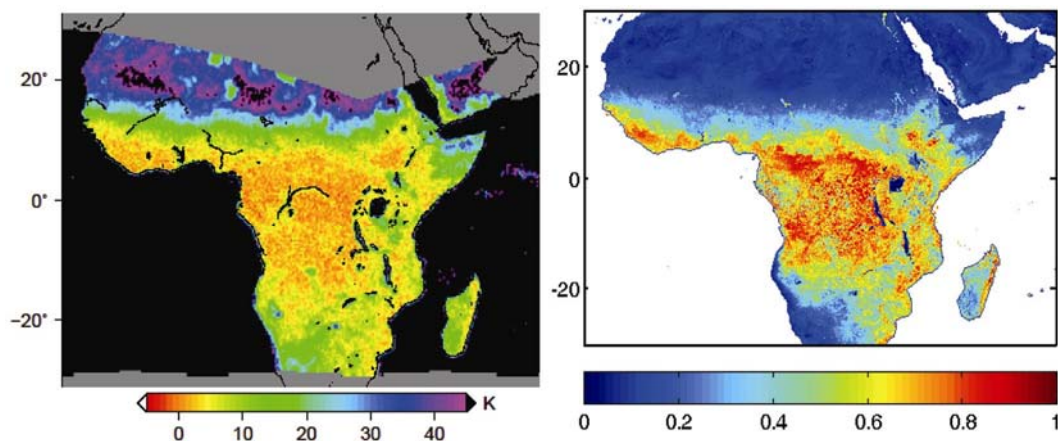


Figure 1. Polarization difference map (18 GHz) over African continent (left panel) and corresponding normalized difference vegetation index (NDVI; right panel).

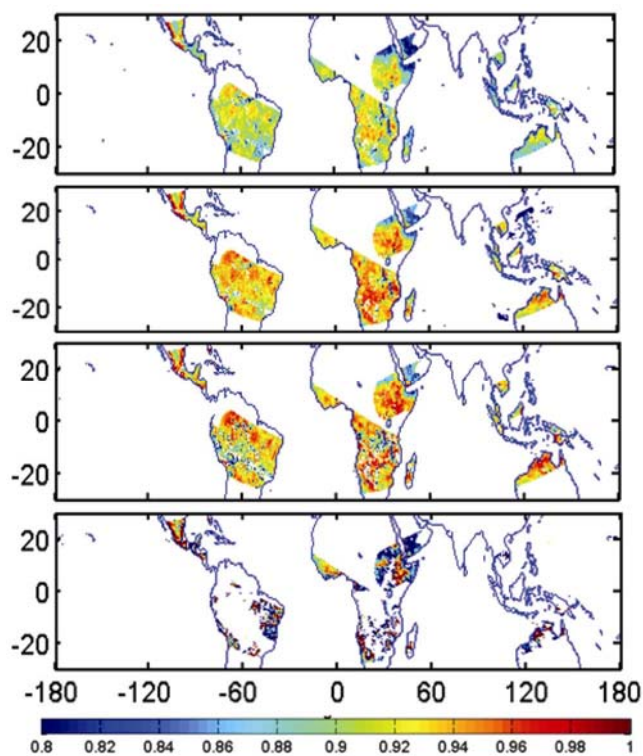


Figure 2. Emissivity maps of MADRAS payload channels at 18, 36, 89 and 157 GHz (first to fourth panel, respectively) at H -polarization.

As vegetation increases the surface becomes more rough, surface scattering increases and it deviates from its specular nature. At higher incidence angle, as the roughness increases, the horizontal component of TB undergoes relatively higher increase than the vertical component and hence the PD decreases with increasing roughness. Further moving towards the southern part of the African desert, the terrain is a transition zone from the desert to the thick tropical vegetation and is dominated by dry and moist savannas. In these regions the NDVI gradually

increases from 0.1 to 0.3 and the corresponding PD decreases from 30 to 10 K. The tropical forest having NDVI of 0.6–0.8, shows low PD with less variation (0–5 K). In general, microwave polarization difference shows a decrease with increasing vegetation¹⁷.

Land surface emissivity of MADRAS frequencies

Satellite-based microwave radiometers receive emission signals from the Earth and the intervening atmosphere. The atmospheric contribution to the radiance measurements is quantified by applying an in-house developed Microwave Radiative Transfer (MRT) computation code on the atmospheric profiles of pressure (P), temperature (T) and relative humidity (RH) and eq. (2) is solved on a pixel basis. The accuracy of this methodology¹⁸ has been extensively examined and validated by (1) comparing with theoretical estimate of emissivity over desert soil condition, (2) comparing with other satellite observation and (3) comparing with emissivity climatology⁵. As the *in situ* measured profiles of atmospheric parameters are not available within the space–time collocation of MT satellite passes, ECMWF/ERA reanalyses data have been used. Stringent cloud screening has been carried out based on collocated SAPHIR data (identify and remove deep convective pixels¹⁹), visual and digital identification of clouds¹⁴ using KALPANA (Visible, IR data) and merged IR TB data (<ftp://disc2.nascom.nasa.gov>) on global basis. ECMWF/ERA reanalyses are the major source of atmospheric and skin temperature data for global emissivity estimation. The emissivity estimation, in this analysis is limited within the time window of ± 1.5 h of reanalyses data time – 0, 6, 12, 18 UTC of the day, in order to reduce the uncertainties in emissivity due to large diurnal variations in T_{skin} over arid and semi-arid regions^{20,21}. The error associated with emissivity determination on a pixel basis depends on skin temperature (error 0.004/K),

Table 1. Emissivity values for different land surface classes. Standard deviations are given in parenthesis

Location	Surface class	18H	18V	37H	37V	89H	89V	157H	157V
160–20°N	Desert (Africa)	0.807	0.945	0.838	0.953	0.855	0.945	0.703	0.832
45–50°E		(0.006)	(0.012)	(0.005)	(0.010)	(0.011)	(0.011)	(0.014)	(0.014)
22–27°N	Desert (USA)	0.901	0.944	0.924	0.956	0.922	0.948	0.928	0.951
100–105°S		(0.009)	(0.003)	(0.008)	(0.003)	(0.005)	(0.003)	(0.007)	(0.009)
5–12°N	Mountain forest	0.925	0.944	0.944	0.959	0.951	0.963	0.899	0.912
35–40°E		(0.015)	(0.012)	(0.021)	(0.010)	(0.024)	(0.008)	(0.051)	(0.055)
11–14°N	Dry savanna	0.894	0.988	0.918	0.992	0.918	0.972	0.845	0.906
25–30°E		(0.002)	(0.003)	(0.002)	(0.002)	(0.004)	(0.004)	(0.016)	(0.018)
5–10°N	Moist savanna	0.919	0.942	0.939	0.955	0.942	0.953	0.798	0.806
25–30°E		(0.003)	(0.002)	(0.002)	(0.002)	(0.002)	(0.001)	(0.077)	(0.079)
8–13°S	Thorn forest	0.909	0.924	0.929	0.939	0.904	0.913	–	–
18–30°E		(0.016)	(0.009)	(0.013)	(0.008)	(0.020)	(0.017)	–	–
0–5°N	Evergreen forest	0.932	0.941	0.944	0.958	0.963	0.943	–	–
60°–70°S		(0.003)	(0.003)	(0.006)	(0.002)	(0.01)	(0.01)	–	–

Table 2. Emissivity climatology (TELSEM database⁵) values averaged for the corresponding land surface classes listed in Table 1. Standard deviations are given in parenthesis (only V polarization is shown here)

Location	Surface class	19V	37V	85V
16–20°N	Desert (Africa)	0.968	0.952	0.935
45–50°E		(0.0002)	(0.0002)	(0.0003)
22–27°N	Desert (USA)	0.975	0.972	0.971
100–105°S		(0.015)	(0.016)	(0.021)
5–12°N	Mountain forest	0.978	0.971	0.970
35–40°E		(0.014)	(0.014)	(0.020)
11–14°N	Dry savanna	0.990	0.981	0.968
25–30°E		(0.016)	(0.016)	(0.017)
5–10°N	Moist savanna	0.979	0.970	0.964
25–30°E		(0.014)	(0.013)	(0.021)
8–13°S	Thorn forest	0.983	0.974	0.973
18–30°E		(0.017)	(0.019)	(0.043)
0–5°N	Evergreen forest	0.978	0.967	0.966
60°–70°S		(0.016)	(0.016)	(0.046)

atmospheric water vapour profile (error varies with surface classes and frequency^{1,18,22}) and atmospheric temperature profile (error ~ 0.002/K).

The emissivity maps derived for 18, 36, 89 and 157 GHz for H-polarization are shown in Figure 2. From the top, panel 1 represents 18 GHz, panel 2 represents 36 GHz, panel 3 represents 89 GHz and panel 4 represents 157 GHz. Very limited pixels on each pass have satisfied the spatio-temporal collocation condition with ECMWF data. Overall, the land surface emissivity varies between 0.8 and 1. Generally, up to 89 GHz emissivity increases with frequency. Over the tropical regions due to the influence of atmospheric water vapour and clouds, very limited pixels have realistic values of emissivity at 157 GHz, even though stringent cloud screening has been applied. Prigent *et al.*²³ pointed out that longer time series of satellite data at higher frequencies (157 GHz) will have to be processed for reasonable estimation of emissivity because of the sensitivity of these frequencies to

water vapour absorption, and special attention has to be given to the accuracy of water vapour profile input and the water vapour absorption model. Different surface classes are discernable from the low-frequency maps. Deserts/semi-arid regions over Africa, Australia and North America show low emissivity values. Very low emissivity values are observed in the desert regions of Arabia. These regions are identified to be composed of sedimentary deposits of quartz, which has higher dielectric constant²⁴ compared to dry soil. Vegetated and forest regions (in Africa and Amazon) have high emissivity values close to 1. The emissivity for different land surface classes for all MADRAS channels (except 22.23 GHz) is given in Table 1. The table also confirms that the emissivity increases with frequency for all the surface classes up to 89 GHz. The region selected for each surface class is nearly uniform as evident from the low values of standard deviation. The derived emissivities have been compared with emissivity climatology values (TELSEM database⁵). This climatology is based on 8 years of Special Sensor Microwave Imager (SSM/I on-board DMSP satellites) monthly mean emissivities at different frequencies (19, 22, 37 and 85 GHz for V- and H-polarization), with a spatial resolution of 0.25° × 0.25° at the equator (equal area grid). The emissivity climatology values and the corresponding standard deviations are averaged for the selected surface classes and are listed in Table 2. The standard deviations are provided in parenthesis. It should be noted that the MADRAS and SSM/I have slightly different frequency channels (18 and 89 GHz in MADRAS, and 19 and 85 GHz in SSM/I). The 157 GHz climatology values are not available. However, it is observed that the emissivities agree well with the climatology values (within the standard deviations).

Comparison between MADRAS and TMI emissivities

The emissivity for TMI frequencies at 19, 21, 37 and 85 GHz is derived for all the TRMM passes on 9 December

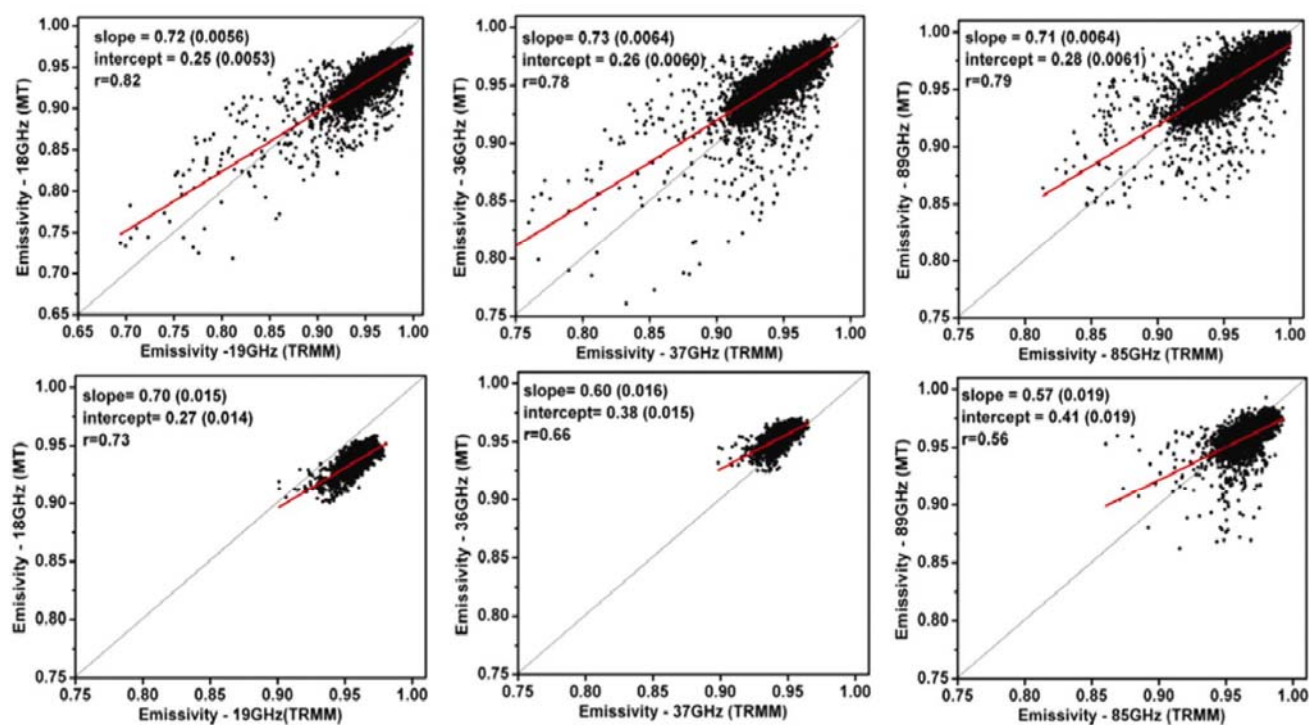


Figure 3. Comparison of emissivity derived from MADRAS and TMI. Emissivity (V -polarization) comparison over a region in Africa (top panel) and that over the Amazon (bottom panel). Grey line represents the 1 : 1 line while the red represent the linear fit.

2011. Owing to random visits of both these satellites and maintaining the ‘time window’ of ± 1.5 h for collocation, only limited continental regions have common coverage in the emissivity maps. Most of the common area available is distributed over tropical forest regions of South America (Amazon) and Africa. A quantitative comparison of emissivity derived from the MADRAS and TMI payloads is carried out using a regression analysis between them for different surface classes. Figure 3 shows the regression between emissivity derived from MADRAS and TMI at 19, 37 and 85 GHz (V -polarization) over Africa (upper panel) and Amazon tropical rainforest (lower panel). Different land surface classes with varying biomass (emissivity value ranging from 0.85 to 0.98) are included in the regression analyses over Africa (upper panel), whereas homogenous tropical forest (Amazon) is analysed over South America.

The regression results (slope ~ 0.7 , intercept ~ 0.2 and correlation coefficient ~ 0.8) show that over Africa emissivities derived from both satellite observations agree well. Almost similar regression results are observed over the Amazon forest. The root mean square difference between the MADRAS and TMI for V -polarization is < 0.02 at 19 GHz and 0.01 at 89 GHz. The results from these analyses based on emissivity estimated for MADRAS frequencies show spectral variation for different surface classes and reasonably good agreement with those derived from TRMM/TMI payload data.

Summary

Data from MADRAS payload of MT obtained on 9 December 2011 have been analysed for various land surface features and to estimate land surface emissivities. Using the dual polarization brightness temperature data from MADRAS, global maps of the polarization difference have been generated. At lower frequencies, the gross and distinct features of the land, namely thick vegetation, deserts and savannas of Africa and Australian grasslands could be clearly discerned. Land surface emissivity maps have been generated for all the MADRAS channels using an in-house developed microwave RT algorithm and are compared with those from the operational TRMM satellite data. Due to the random visits of these two satellites, the space–time collocated data are limited. Despite this, it has been found that the difference in the emissivity estimates from the two satellites is in agreement within a mean difference of 0.02. A consolidated conclusion demands the analysis of a reasonable data volume.

1. Prigent, C., Rossow, W. B. and Mathews, E., Microwave land surface emissivities estimated from SSM/I observations. *J. Geophys. Res. D*, 1997, **102**, 21867–21890.
2. Weng, F., Yan, B. and Grody, N. C., A microwave land emissivity model. *J. Geophys. Res. D*, 2001, **106**, 20115–20123.
3. Jones, A. S. and Haar, H. T. V., Passive microwave remote sensing of cloud liquid water over land regions. *J. Geophys. Res.*, 1990, **95**, 16673–16683.

4. Prigent, C., Aires, F. and Rossow, W. B., Land surface microwave emissivities over the globe for a decade. *Bull. Am. Meteorol. Soc.*, 2006, **87**, 1573–1584.
5. Aires, F., Prigent, C., Bernardo, F., Jiménez, C., Saunders, R. and Brunel, P., A tool to estimate land-surface emissivities at microwave frequencies (TELSEM) for use in numerical weather prediction. *Q. J. R. Meteorol. Soc.*, 2011, **137**, 690–699.
6. Karbou, F., Prigent, C., Eymard, L. and Pardo, J. R., Microwave land emissivity calculations using amsu measurements. *IEEE Trans. Geosci. Remote Sensing*, 2005, **43**, 948–959.
7. Papa, F., Prigent, C., Durand, F. and Rossow, W. B., Wetland dynamics using a suite of satellite observations: A case study of application and evaluation for Indian subcontinent. *Geophys. Res. Lett.*, 2006, **33**, L08401.
8. Kummerow, C. *et al.*, The status of the Tropical Rainfall Measuring Mission (TRMM) after two years in orbit. *J. Appl. Meteorol.*, 2000, **36**, 1965–1982.
9. Meeks, M. L. and Lilley, A. E., The microwave spectrum of oxygen in the earth's atmosphere. *J. Geophys. Res.*, 1963, **68**, 1683–1703.
10. Rosenkranz, P. W., Shape of the 5 mm oxygen band in the atmosphere. *IEEE Trans. Antennas Propag.*, 1975, **AP-23**, 498–506.
11. Ulaby, F. T., Moore, R. K. and Fung, A. K., *Microwave Remote Sensing, Active and Passive*, Addison-Wesley publishing company, 1982, vol. 2.
12. Waters, J. W., Absorption and emission of microwave radiations by atmospheric gases. In *Methods of Experimental Physics*, Academic Press, 1976, vol. 12.
13. Gaut, N. E. and Reifenstein, E. C., Technical Report No. 13, Environmental Research and Technology Inc., Massachusetts, 1971.
14. Meenu, S., Rajeev, K., Parameswaran, K. and Nair, A. K. M., Regional distribution of deep clouds and cloud top altitudes over the Indian subcontinent and the surrounding oceans. *J. Geophys. Res.*, 2010, **115**.
15. Uppala, S. M. *et al.*, The ERA-40 re-analysis. *Q. J. R. Meteorol. Soc.*, 2005, **131**, 2961–3012, doi: 10.1256/qj.04.176.
16. Kummerow, C., Olson, W. S. and Giglio, L., A simplified scheme for obtaining precipitation and vertical hydrometeor profiles from passive microwave sensors. *IEEE Trans. Geosci. Remote Sensing*, 1996, **34**, 1213–1232.
17. Prigent, C., Aires, F., Rossow, W. B. and Matthews, E., Joint characterization of vegetation by satellite observations from visible to microwave wavelengths: a sensitivity analysis. *J. Geophys. Res. D*, 2001, **106**, 20665–20685.
18. Saha, K., Suresh Raju, C., Antony, T. and Krishna Moorthy, K., Land-surface microwave emissivity map of Indian region: Megha-Tropiques perspective. In IEEE Applied Electromagnetics Conference, AEMC 2009, Paper No. WPR-3-7807, 2009, Special Issue – PIER Journal-B and Electromagnetic, 2010.
19. Hong, G., Heygster, G., Miao, J. and Kunzi, K., Detection of tropical deep convective clouds from AMSU-B water vapour channels measurements. *J. Geophys. Res.*, 2005, **110**, D05205, doi: 10.1029/2004JD004949.
20. Grody, N. C. and Weng, F., Microwave emission and scattering from deserts: theory compared with satellite measurements. *IEEE Trans. Geosci. Remote Sensing*, 2008, **46**, 317–319.
21. Prigent, C., Rossow, W., Matthews, E. and Marticorena, B., Microwave radiometric signatures of different surface types in deserts. *J. Geophys. Res. D*, 1999, **104**, 12147–12158.
22. Yang, H. and Weng, F., Error sources in remote sensing of microwave land surface emissivity. *IEEE Trans. Geosci. Remote Sensing*, 2011, **49**, 9.
23. Prigent, C., Wigneron, J. P., Rossow, W. B. and Pardo, J. R., Frequency and angular variations of land surface microwave emissivities: can we estimate SSM/T and AMSU emissivities from SSM/I emissivities? *IEEE Trans. Geosci. Remote Sensing*, 2000, **38**, 2373–2386.
24. Prigent, C., Munier, J. M. and Thomas, B., Microwave signatures over carbonate sedimentary platforms in arid areas: potential geological applications of passive microwave observations. *J. Geophys. Res. Lett.*, 2005, **32**, doi: 10.1029/2005GL024691, 23405.

ACKNOWLEDGEMENTS. We thank Prof. J. Srinivasan, Indian Institute of Science, Bangalore, for valuable discussions and Dr Tapan Misra, Deputy Director, Space Applications Centre (SAC), Ahmedabad, for discussion on technical aspects of MADRAS radiometer. We also thank MOSDAC, SAC, for supplying the satellite data (MT and KALPANA data); <http://mirador.gsfc.nasa.gov> for TRMM/TMI data, <http://dataportal.ecmwf.in/data/d/interimdaily> for ECMWF reanalysis data and www.laadsweb.nascom.gov for MODIS NDVI data. T.A. thanks ISRO for funds as part of the Ph D programme.